Phase transitions between different spin-glass phases and between different chaoses in quenched random chiral systems

Tolga Çağlar[1] and A. Nihat Berker[2,3,*]

[1]*Faculty of Engineering and Natural Sciences, Sabancı University, Tuzla, Istanbul 34956, Turkey*

[2]*Faculty of Engineering and Natural Sciences, Kadir Has University, Cibali, Istanbul 34083, Turkey*

[3]*Department of Physics, Massachusetts Institute of Technology, Cambridge, Massachusetts 02139, USA*

(Received 14 June 2017; revised manuscript received 20 August 2017; published 5 September 2017)

The left-right chiral and ferromagnetic-antiferromagnetic double-spin-glass clock model, with the crucially even number of states $q = 4$ and in three dimensions $d = 3$, has been studied by renormalization-group theory. We find, for the first time to our knowledge, four spin-glass phases, including conventional, chiral, and quadrupolar spin-glass phases, and phase transitions between spin-glass phases. The chaoses, in the different spin-glass phases and in the phase transitions of the spin-glass phases with the other spin-glass phases, with the non-spin-glass ordered phases, and with the disordered phase, are determined and quantified by Lyapunov exponents. It is seen that the chiral spin-glass phase is the most chaotic spin-glass phase. The calculated phase diagram is also otherwise very rich, including regular and temperature-inverted devil's staircases and reentrances.

DOI: 10.1103/PhysRevE.96.032103

I. INTRODUCTION

Spin-glass phases, created by competing frustrated random ferromagnetic and antiferromagnetic interactions, have been known [1] to incorporate a plethora of interesting complex phenomena, not the least being the natural generation chaos [2–4]. Recently, it has been shown [5,6] that competing left- and right-chiral interactions also create spin-glass phases, even in the absence of competing ferromagnetic and antiferromagnetic interactions. First shown [5] with the chiral Potts models [7–11] with the inclusion of quenched randomness, chiral spin glasses were recently extended [6] to clock models with an odd number of states ($q = 5$), resulting in a literally moviesque sequence of phase diagrams, including regular and inverted devil's staircases, a chiral spin-glass phase, and algebraic order.

The chiral clock model work was purposefully initiated [6] with an odd number of states q, in order to deal with the complexity of the global phase diagram, since it is known that odd-q models do not show [12] the traditional ferromagnetic-antiferromagnetic spin-glass phase. This is because neighboring antiferromagnetically interacting odd-q clock spins cannot achieve perfect antiferromagnetic alignment. Furthermore, there are two configurations for the near-antiferromagnetic alignment, creating a built-in disorder. The traditional ferromagnetic-antiferromagnetic spin-glass phase does not occur and the antiferromagnetic phase is a critical phase lacking conventional long-range order [12]. On the other hand, the even-q clock spins can achieve complete antiferromagnetic pairing and exhibit the conventional antiferromagnetic long-range order and the traditional ferromagnetic-antiferromagnetic spin-glass phase [13]. Thus, the current study is on the random chiral clock model with an even number of states ($q = 4$), which supports the ferromagnetic-antiferromagnetic usual spin-glass phase [13], as well as, as we see below, with added phase diagram complexity, the chiral spin-glass phase and two other new spin-glass phases. A double spin-glass model is constructed, including competing quenched random left-right chiral and ferromagnetic-antiferromagnetic interactions and solved in three dimensions by renormalization-group theory.

The extremely rich phase diagram includes, to our knowledge for the first time, more than one (four) spin-glass phases in the same phase diagram and three separate spin-glass–to–spin-glass phase transitions. These constitute phase transitions between chaoses. We determine the chaotic behaviors of the spin-glass phases, of the phase transitions between the spin-glass phases, and the phase transitions between the spin-glass phases and the ferromagnetic, antiferromagnetic, quadrupolar, and disordered phases.

II. DOUBLE SPIN-GLASS SYSTEM: LEFT-RIGHT CHIRAL AND FERRO-ANTIFERRO INTERACTIONS

The q-state clock spin glass is composed of unit spins that are confined to a plane and that can only point along q angularly equidistant directions, with Hamiltonian

$$-\beta\mathcal{H} = \sum_{\langle ij\rangle} J_{ij}\vec{s}_i \cdot \vec{s}_j = \sum_{\langle ij\rangle} J_{ij}\cos\theta_{ij}, \tag{1}$$

where $\beta = 1/k_BT$, $\theta_{ij} = \theta_i - \theta_j$, at each site i the spin angle θ_i takes on the values $(2\pi/q)\sigma_i$ with $\sigma_i = 0,1,2,\ldots,(q-1)$, and $\langle ij\rangle$ denotes summation over all nearest-neighbor pairs of sites. As the long-studied ferromagnetic-antiferromagnetic spin-glass system [1], the bond strengths J_{ij}, with quenched (frozen) ferromagnetic-antiferromagnetic randomness, are $+J > 0$ (ferromagnetic) with probability $1 - p$ and $-J$ (antiferromagnetic) with probability p, with $0 \leqslant p \leqslant 1$. Thus, the ferromagnetic and antiferromagnetic interactions locally compete in frustration centers. Recent studies on ferromagnetic-antiferromagnetic clock spin glasses are reported in Refs. [12–14].

In the q-state chiral clock double spin glass, recently introduced (and used in the qualitatively different odd $q = 5$), frustration also occurs via randomly frozen left or right

*nihatberker@khas.edu.tr

chirality [5], thus doubling the spin-glass mechanisms. The Hamiltonian in Eq. (1) is generalized to random local chirality,

$$-\beta\mathcal{H} = \sum_{\langle ij\rangle}\left[J_{ij}\cos\theta_{ij} + \Delta\,\delta\left(\theta_{ij} + \eta_{ij}\frac{2\pi}{q}\right)\right]. \quad (2)$$

In a cubic lattice, as sites along the respective coordinate directions are considered, the x, y, or z coordinates increase. Since bond moving in the Migdal-Kadanoff approximation [15,16] is done transversely to the bond directions, this sequencing is respected. Equivalently, in the corresponding hierarchical lattice [17–21], one can always define a direction along the connectivity, for example, from left to right, and assign consecutive increasing number labels to the sites. In Eq. (2), for each pair of nearest-neighbor sites $\langle ij\rangle$ the numerical site label j is ahead of i, frozen (quenched) $\eta_{ij} = 1$ (left chirality) or -1 (right chirality), and the delta function $\delta(x) = 1\,(0)$ for $x = 0\,(x \neq 0)$. The overall concentrations of left and right chirality are, respectively, $1-c$ and c, with $0 \leqslant c \leqslant 1$. The strength of the random chiral interaction is Δ/J, with the temperature divided out. Thus, the system is chiral for $\Delta \neq 0$, chiral-symmetric for $c = 0.5$, and chiral-symmetry-broken for $c \neq 0.5$. The global phase diagram is in terms of temperature J^{-1}, antiferromagnetic bond concentration p, random chirality strength Δ/J, and chiral symmetry-breaking concentration c.

III. RENORMALIZATION-GROUP METHOD: MIGDAL-KADANOFF APPROXIMATION AND EXACT HIERARCHICAL LATTICE SOLUTION

Our method, previously described in extensive detail [6] and used on a qualitatively different model with qualitatively different results, is simultaneously the Migdal-Kadanoff approximation [15,16] for the cubic lattice and the exact solution [17–21] for a $d = 3$ hierarchical lattice, with length rescaling factor $b = 3$. Exact calculations on hierarchical lattices are also currently widely used in a variety of statistical mechanics [22–36], finance [37], and, most recently, DNA-binding [38] problems.

Under the renormalization-group transformation [6], the Hamiltonian, Eq. (2), maps onto the more general form

$$-\beta\mathcal{H} = \sum_{\langle ij\rangle} V_{ij}(\theta_{ij}), \quad (3)$$

where $\theta_{ij} = \theta_i - \theta_j$ can take $q = 4$ values, so that for each pair $\langle ij\rangle$ of nearest-neighbor sites, there are $q = 4$ different interaction constants

$$\{V_{ij}(\theta_{ij})\} = \{V_{ij}(0), V_{ij}(\pi/2), V_{ij}(\pi), V_{ij}(3\pi/2)\} \equiv \mathbf{V}_{ij}, \quad (4)$$

which are, in general, different at each locality (quenched randomness). The largest element of $\{V_{ij}(\theta_{ij})\}$ at each locality $\langle ij\rangle$ is set to 0, by subtracting the same constant from all $q = 4$ interaction constants, with no effect on the physics; thus, the $q - 1 = 3$ other interaction constants are negative.

The starting double-bimodal quenched probability distribution of the interactions, characterized by p and c as described above, is not conserved under rescaling. The renormalized quenched probability distribution of the interactions is obtained by the convolution [39]

$$P'(\mathbf{V}'_{i'j'}) = \int\left\{\prod_{ij}^{i'j'} d\mathbf{V}_{ij}\,P(\mathbf{V}_{ij})\right\}\delta(\mathbf{V}'_{i'j'} - \mathbf{R}(\{\mathbf{V}_{ij}\})), \quad (5)$$

where $\mathbf{V}_{ij} \equiv \{V_{ij}(\theta_{ij})\}$ as in Eq. (4), $\mathbf{R}(\{\mathbf{V}_{ij}\})$ represents the renormalization-group recursion relation [6], primes refer to the renormalized system, and the procedure is effected numerically. The different phases and phase transitions of the system are identified by the different asymptotic renormalization-group flows of the quenched probability distribution $P(\mathbf{V}_{ij})$. Similar previous studies, on other spin-glass systems, are reported in Refs. [12,13,40–47].

IV. GLOBAL PHASE DIAGRAM: MULTIPLE-SPIN-GLASS PHASES

Figure 1 shows a calculated sequence of phase diagram cross sections for the left-chiral ($c = 0$) (top row) and quenched random left- and right-chiral ($c = 0.5$) (bottom row) systems with, in both cases, quenched random ferromagnetic and antiferromagnetic interactions. The system exhibits a disordered phase (D), a ferromagnetic phase (F), a conventionally ordered (in contrast to the algebraically ordered for $q = 5$) antiferromagnetic phase (A), a quadrupolar phase (Q), a new "one-step" phase (R), a multitude of different chiral phases, and four spin-glass phases ($\mathrm{S_{Ch}}, \mathrm{S_{FA}}, \mathrm{S}_Q, \mathrm{S}_R$) including spin-glass–to–spin-glass phase transitions. The ferromagnetic and different chiral phases accumulate as conventional and temperature-inverted (abutting to the reentrant [48–52] disordered phase) devil's staircases [53,54] at their boundary with the disordered (D) phase. This accumulation and its multiplicity of intervening phases occur at all scales of phase diagram space (i.e., at all magnifications of the phase diagram figure, as, for example, shown up to a 100-fold calculated magnification in Fig. 4 of [6]), which is the definition of a devil's staircase.

Unlike the odd-q case of $q = 5$, which incorporates built-in entropy [6] even without any quenched randomness, no algebraically ordered phase [55,56] occurs in this even-q case of $q = 4$. The devil's staircase of the chiral phases is again seen. Most interestingly, quadrupolar and "one-step" phases, different spin-glass phases for the first time in the same phase diagram, and spin-glass–to–spin-glass direct phase transitions are seen. The phases and phase boundaries involving spin glassiness are tracked through the calculated Lyapunov exponents of their chaos.

In all ordered phases, the renormalization-group trajectories flow to strong (infinite) coupling. In the ferromagnetic phase, under renormalization-group transformations, the interaction $V_{ij}(0)$ becomes asymptotically dominant. In the antiferromagnetic phase, under renormalization-group transformations, the interaction $V_{ij}(\pi)$ becomes asymptotically dominant. In the quadrupolar phase Q, the interactions $V_{ij}(0)$ and $V_{ij}(\pi)$ become asymptotically dominant and equal. Thus, there are two such quadrupolar phases, namely, along the spin directions $\pm x$ and $\pm y$, with the additional (factorized) trivial degeneracy of a $\pm$ spin direction at each site. In the new "one-step phase" R, the interactions $V_{ij}(+\pi/2)$ and $V_{ij}(-\pi/2)$ become

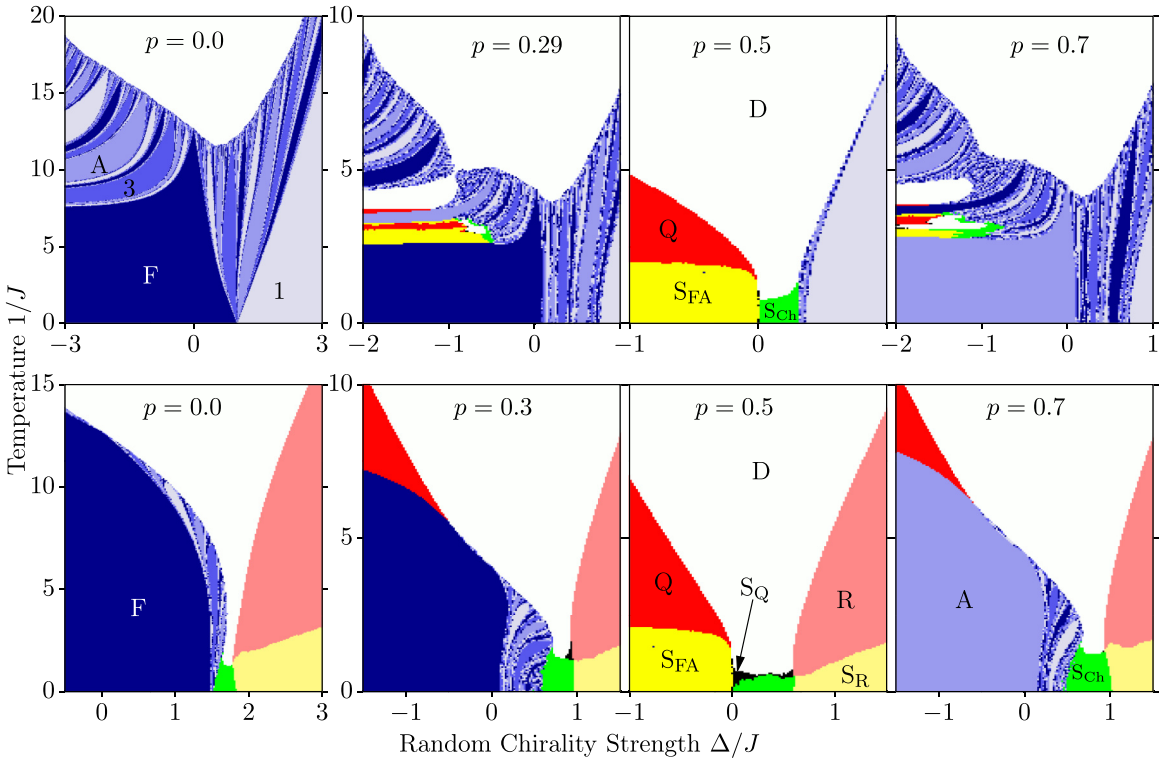

FIG. 1. A calculated sequence of phase diagrams for the left chiral ($c = 0$) (top row) and quenched random left and right chiral ($c = 0.5$) (bottom row) systems with, in both cases, quenched random ferromagnetic and antiferromagnetic interactions. The horizontal axis is the random chirality strength Δ/J. The consecutive phase diagrams are for different concentrations p of antiferromagnetic interactions. The system exhibits a ferromagnetic phase F, an antiferromagnetic phase A, a multitude of different chiral phases, a quadrupolar phase Q, a "one-step" phase R, and four differently ordered spin-glass phases: the chiral spin-glass S_{Ch}, the usual ferromagnetic-antiferromagnetic spin glass S_{FA}, the quadrupolar spin glass S_Q, and S_R. The phase diagrams obtained from p and $1 - p$ are symmetric, since the system has an even number of spin directions. For some of the chiral phases, the $\pi/2$ multiplicity of the asymptotically dominant interaction is indicated. The ferromagnetic and chiral phases accumulate as different devil's staircases at their boundary with the disordered (D) phase.

asymptotically dominant and equal. Thus, in this phase, the average local spins can span all spin directions, taking $\pm\pi/2$ steps from one spin to the next in the renormalized systems. The identification of the distinct chiral phases, each with distinct chiral pitches, has been explained in Ref. [6].

The renormalization-group trajectories starting in the spin-glass phases, unlike those in the ferromagnetic, antiferromagneric, quadrupolar, "one-step," and chiral phases, do not have the asymptotic behavior where at any scale one potential $V(\theta)$ is dominant. These trajectories of the spin-glass phases asymptotically go to a strong-coupling fixed probability distribution $P(\mathbf{V}_{ij})$ which assigns nonzero probabilities to a distribution of $\mathbf{V}_{ij}$ values, with no single $V_{ij}(\theta)$ being dominant. These distributions are shown in Figs. 2 and 3. Different asymptotic fixed probability distributions indicate different spin-glass phases.

Since, at each locality, the largest interaction in $\{V_{ij}(0), V_{ij}(\pi/2), V_{ij}(\pi), V_{ij}(3\pi/2)\}$ is set to 0 and the three other interactions are thus made negative, by subtracting the same constant from all four interactions without affecting the physics, the quenched probability distribution $P(\mathbf{V}_{ij})$, a function of four variables, is actually composed of four functions $P_\sigma(\mathbf{V}_{ij})$ of three variables, each such function

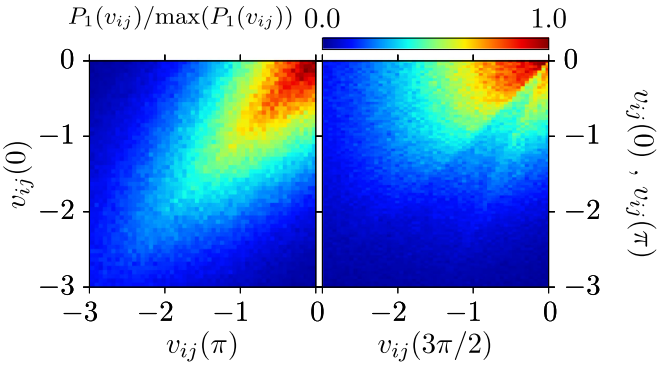

FIG. 2. Asymptotic fixed distribution of the chiral spin-glass phase S_{Ch}. The part of the fixed distribution $P_1(\mathbf{V}_{ij})$, for interactions $\mathbf{V}_{ij}$ in which $V_{ij}(\pi/2)$ is maximum and therefore 0 (and the other three interactions are negative), is shown in this figure, with $v_{ij}(\theta) = V_{ij}(\theta)/\langle|V_{ij}(\theta)|\rangle$. The projections of $P_1(\mathbf{V}_{ij})$ onto two of its three arguments are shown in each panel. The other three $P_\sigma(\mathbf{V}_{ij})$ have the same fixed distribution. Thus chirality is broken locally but not globally, just as, in the long-time studied ferromagnetic-antiferromagnetic spin glasses, spin-direction symmetry breaking is local but not global (i.e., the local magnetization is nonzero and the global magnetization is 0).

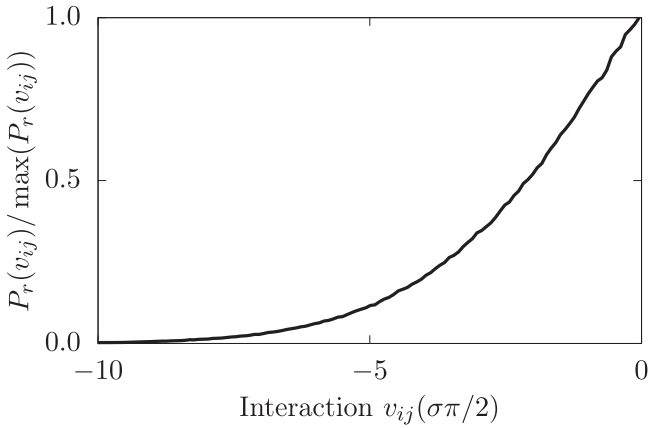

FIG. 3. Asymptotic fixed distributions of three spin-glass phases, with $v_{ij}(\theta) = V_{ij}(\theta)/\langle|V_{ij}(\theta)|\rangle$. For the ferromagnetic-antiferromagnetic spin-glass S_{FA} phase, $r = 0, \sigma = 2$ and $r = 2, \sigma = 0$. The other two angles do not occur. For the quadrupolar spin-glass S_Q phase, $r = 0, \sigma = 1$ and $r = 1, \sigma = 0$, with $V_{ij}(0) = V_{ij}(\pi)$ and $V_{ij}(\pi/2) = V_{ij}(3\pi/2)$. For the spin-glass S_R phase, $r = 1, \sigma = 3$ and $r = 3, \sigma = 1$. The other two angles do not occur. The $v_{ij}(0) = v_{ij}(\pi)$ curve, obtained from the left panel in Fig. 2, also matches the curve here.

corresponding to one of the interactions being 0 and the other three, arguments of the function, being negative. Figures 2 and 3 show the latter functions.

In Fig. 2 for the spin-glass phase S_{Ch}, the part of the fixed distribution, $P_1(\mathbf{V}_{ij})$, for the interactions $\mathbf{V}_{ij}$ in which $V_{ij}(\pi/2)$ is maximum and therefore 0 (and the other three interactions are negative) is shown. The projections of $P_1(\mathbf{V}_{ij})$ onto two of its three arguments are shown in each panel in Fig. 2. The other three $P_\sigma(\mathbf{V}_{ij})$ have the same fixed distribution. Thus, chirality is broken locally, but not globally, just as, in the long-time-studied ferromagnetic-antiferromagnetic spin glasses, spin-direction symmetry breaking is local but not global (i.e., the local magnetization is nonzero and the global magnetization is 0). The asymptotic fixed distribution of the phase S_{Ch}, shown in Fig. 2, assigns nonzero probabilities to a continuum of values for all four interactions $\{V_{ij}(0), V_{ij}(\pi/2), V_{ij}(\pi), V_{ij}(3\pi/2)\}$. The phase S_{Ch} is therefore a chiral spin-glass phase. The similar chiral spin-glass phase has been seen previously, but as the sole spin-glass phase, for the odd $q = 5$ [6]. The chiral spin-glass phase occurs even when there are no competing ferromagnetic-antiferromagnetic interactions [5,6].

As shown in Fig. 3, in the asymptotic fixed distribution of the spin-glass phase S_{FA}, nonzero probabilities are assigned to a continuum of values of $\{V_{ij}(0), V_{ij}(\pi)\}$. Figure 3 shows the fixed distribution values $P_0(V_{ij}(\pi))$ for $V_{ij}(0)$ maximum and therefore set to 0. Completing the asymptotic fixed distribution of S_{FA} is an identical function $P_2(V_{ij}(0))$ for $V_{ij}(\pi)$ maximum and therefore set to 0. At this fixed distribution, the values of $V_{ij}(\pi/2)$ and $V_{ij}(3\pi/2)$ diverge to $-\infty$, so that these angles do not occur. Thus, S_{FA} is the long-studied [1] spin-glass phase of competing ferromagnetic and antiferromagnetic interactions.

Figure 3 also shows the asymptotic fixed distribution of the spin-glass phase S_R, with the functions $P_1(V_{ij}(3\pi/2))$ for $V_{ij}(\pi/2)$ maximum (and therefore set to 0) and $P_3(V_{ij}(\pi/2))$ for $V_{ij}(3\pi/2)$ maximum (and therefore set to 0). Again, the other two angles do not occur at this asymptotic fixed distribution. Furthermore, Fig. 3 also shows the asymptotic fixed distribution of the spin-glass phase S_Q, with the functions $P_0(V_{ij}(\pi/2))$ and $P_1(V_{ij}(0))$, with $V_{ij}(0) = V_{ij}(\pi)$ and $V_{ij}(\pi/2) = V_{ij}(3\pi/2)$. Thus, this fixed distribution does not locally distinguish between $\pm$ spin directions and is thus a quadrupolar spin-glass phase.

In fact, the $v_{ij}(0) = v_{ij}(\pi)$ curve obtained from the left panel in Fig. 2 also matches the curve here. The three fixed distributions given in Fig. 3 exhibit the same numerical curve but refer to widely different interactions. Thus, they underpin different spin-glass phases.

V. PHASE TRANSITIONS BETWEEN CHAOS

Another distinctive mechanism, that of chaos under scale change [2–4] or, equivalently [13], chaos under spatial translation, occurs within the spin-glass phase and differently at the spin-glass phase boundary [13] in systems with competing ferromagnetic and antiferromagnetic interactions [2–4,13,46,57–83] and, more recently, with competing left- and right-chiral interactions [5,6]. Originally found in hierarchical systems [2–4], scaling or, equivalently, translation spin-glass chaos is now well accepted for real $d = 3$ lattices and experimental systems [2–4,13,46,57–83].

Figure 4 gives the asymptotic chaotic renormalization-group trajectories of the four spin-glass phases and of the phase boundaries of the spin-glass phases with the other spin-glass phases, the non-spin-glass ordered phases, and the disordered phase.

Chaos is measured by the Lyapunov exponent, whose calculation for the multi-interaction $V_{ij}(0)$, $V_{ij}(\pi/)$, $V_{ij}(\pi)$, $V_{ij}(3\pi/2)$ case is given in Ref. [6]. Spin-glass chaos occurs for $\lambda > 0$ [74], and the more positive λ, the stronger is chaos. Within all four spin-glass phases, the average interaction diverges as $\langle|V|\rangle \sim b^{y_R n}$, where n is the number of renormalization-group iterations and $y_R = 0.25$ is the runaway exponent. In the non-spin-glass ordered phases, the runaway exponent value is $y_R = d - 1 = 3$ [84].

At the S_{Ch}-S_R, S_{Ch}-S_Q, and S_{FA}-F and its symmetric S_{FA}-A phase boundaries, $y_R = 0.25$ also. At the S_{Ch}-S_{FA} phase boundary, $y_R = 0.11$ for $V_{ij}(0)$, $V_{ij}(\pi)$, and $y_R = 0.25$ for $V_{ij}(\pi/2)$, $V_{ij}(3\pi/2)$. At the phase boundaries of the spin-glass phases with some non-spin-glass ordered and disordered phases, the average interaction remains nondivergent, fixed at $\langle V\rangle = -0.34$ for S_{FA}-Q, S_R-R, S_Q-D and $\langle V\rangle = -1.07$ for S_{Ch}-D. As indicated by the Lyapunov exponents, chaos is stronger within the spin-glass phase than at its phase boundaries with non-spin-glass phases.

As expected from the asymptotic fixed distribution analysis given above, the three spin-glass phases S_{FA}, S_Q, and S_R and the phase transitions between these phases have the same Lyapunov exponent, $\lambda = 1.92$, and therefore the same degree of chaos. The chiral spin-glass S_{Ch} has more chaos ($\lambda = 1.98$) from the other three spin-glass phases. The phase transition between the chiral spin-glass phase S_{Ch} and the other three spin-glass phases is a phase transition between different types

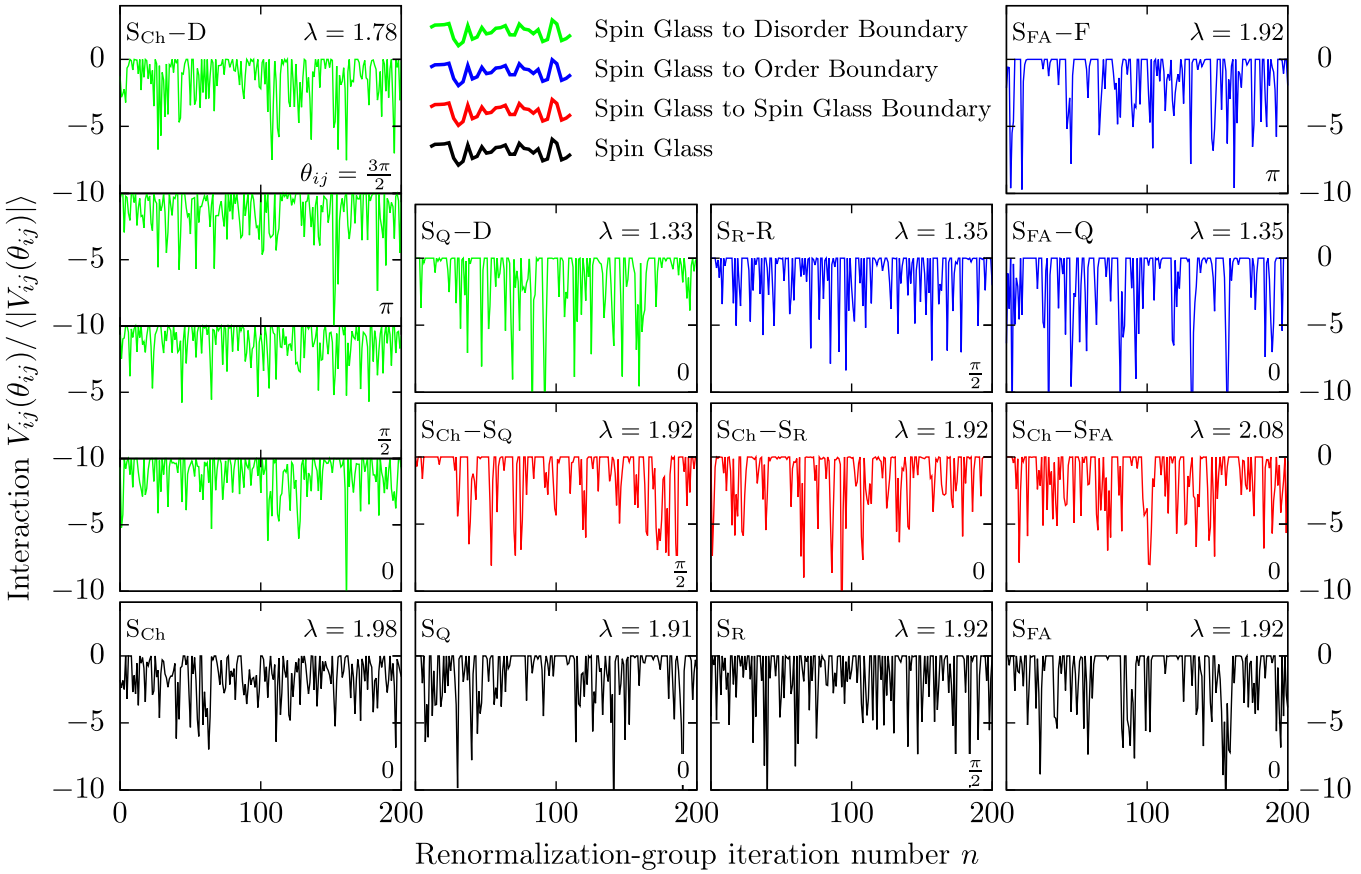

FIG. 4. Chaotic renormalization-group trajectories of the four spin-glass phases (black) and of the phase boundaries of the spin-glass phases with other spin-glass phases (red) and with non-spin-glass ordered (blue) and disordered (green) phases. The phase boundary chaoses of each spin-glass phase are given in the corresponding vertically aligned panels. In each case, only one of the four interactions $V_{ij}(0)$, $V_{ij}(\pi/2)$, $V_{ij}(\pi)$, and $V_{ij}(3\pi/2)$ at a given location $\langle ij\rangle$, under consecutive renormalization-group transformations, is shown, except, for illustration, all four interactions are shown for the chaos at the phase transition between the chiral spin-glass and disordered phases. The θ_{ij} angular value of each interaction $V_{ij}(\theta_{ij})$ is indicated in the panels, as well as the Lyapunov exponent λ calculated from the chaotic sequence under renormalization-group transformations. The Lyapunov exponent is calculated over 1000 renormalization-group iterations, after throwing out the first 200 iterations. Within all four spin-glass phases, the average interaction diverges as $\langle|V|\rangle \sim b^{y_R n}$, where n is the number of renormalization-group iterations and $y_R = 0.25$ is the runaway exponent. At the S_{Ch}-S_R, S_{Ch}-S_Q, S_{FA}-A, and S_{FA}-F phase boundaries, $y_R = 0.25$ also. At the S_{Ch}-S_{FA} phase boundary, $y_R = 0.11$ for $V_{ij}(0)$, $V_{ij}(\pi)$ and $y_R = 0.25$ for $V_{ij}(\pi/2)$, $V_{ij}(3\pi/2)$. At the phase boundaries of the spin-glass phases with some non-spin-glass-ordered and disordered phases, the average interaction remains nondivergent, fixed at $\langle V\rangle = -0.34$ for S_{FA}-Q, S_R-R, S_Q-D and $\langle V\rangle = -1.07$ for S_{Ch}-D. As indicated by the Lyapunov exponents, chaos is stronger within the chiral spin-glass phase.

of chaos. This phase transition itself of course exhibits chaos, as do all spin-glass phase boundaries.

VI. CONCLUSION

The left-right chiral and ferromagnetic-antiferromagnetic double spin-glass clock model, with the crucially even number of states $q = 4$ and in three dimensions $d = 3$, has been solved by renormalization-group theory, which is approximate for the cubic lattice and exact for the corresponding hierarchical lattice. We find in the same phase diagram, for the first time to our knowledge, four spin-glass phases, including conventional, chiral, and quadrupolar spin-glass phases and phase transitions between spin-glass phases. The chaoses, in the different spin-glass phases and in the phase transitions of the spin-glass phases with the other spin-glass phases, the non-spin-glass ordered phases, and the disordered phase, are determined and quantified by Lyapunov exponents. It is seen that the chiral spin-glass phase is the most chaotic spin-glass phase. The calculated phase diagram is also otherwise very rich, including regular and temperature-inverted devil's staircases and reentrances.

The recently found chiral spin-glass phase could possibly be seen in quenched random dimolecular crystals. In fact, if magnetic moments could be included in the component chiral molecules, the double spin-glass system, with the multiplicity of spin-glass phases seen here, could be achieved.

ACKNOWLEDGMENT

Support from the Academy of Sciences of Turkey (TÜBA) is gratefully acknowledged.

[1] H. Nishimori, *Statistical Physics of Spin Glasses and Information Processing* (Oxford University Press, Oxford, UK, 2001).
[2] S. R. McKay, A. N. Berker, and S. Kirkpatrick, Phys. Rev. Lett. **48**, 767 (1982).
[3] S. R. McKay, A. N. Berker, and S. Kirkpatrick, J. Appl. Phys. **53**, 7974 (1982).
[4] A. N. Berker and S. R. McKay, J. Stat. Phys. **36**, 787 (1984).
[5] T. Çağlar and A. N. Berker, Phys. Rev. E **94**, 032121 (2016).
[6] T. Çağlar and A. N. Berker, Phys. Rev. E **95**, 042125 (2017).
[7] S. Ostlund, Phys. Rev. B **24**, 398 (1981).
[8] M. Kardar and A. N. Berker, Phys. Rev. Lett. **48**, 1552 (1982).
[9] D. A. Huse and M. E. Fisher, Phys. Rev. Lett. **49**, 793 (1982).
[10] D. A. Huse and M. E. Fisher, Phys. Rev. B **29**, 239 (1984).
[11] R. G. Caflisch, A. N. Berker, and M. Kardar, Phys. Rev. B **31**, 4527 (1985).
[12] E. Ilker and A. N. Berker, Phys. Rev. E **90**, 062112 (2014).
[13] E. Ilker and A. N. Berker, Phys. Rev. E **87**, 032124 (2013).
[14] C. Lupo and F. Ricci-Tersenghi, Phys. Rev. B **95**, 054433 (2017).
[15] A. A. Migdal, Zh. Eksp. Teor. Fiz. **69**, 1457 (1975) [Sov. Phys. JETP **42**, 743 (1976)].
[16] L. P. Kadanoff, Ann. Phys. (NY) **100**, 359 (1976).
[17] A. N. Berker and S. Ostlund, J. Phys. C **12**, 4961 (1979).
[18] R. B. Griffiths and M. Kaufman, Phys. Rev. B **26**, 5022R (1982).
[19] M. Kaufman and R. B. Griffiths, Phys. Rev. B **30**, 244 (1984).
[20] S. R. McKay and A. N. Berker, Phys. Rev. B **29**, 1315 (1984).
[21] M. Hinczewski and A. N. Berker, Phys. Rev. E **73**, 066126 (2006).
[22] B. Derrida and G. Giacomin, J. Stat. Phys. **154**, 286 (2014).
[23] M. F. Thorpe and R. B. Stinchcombe, Philos. Trans. Roy. Soc. A **372**, 20120038 (2014).
[24] A. Efrat and M. Schwartz, Physica **414**, 137 (2014).
[25] C. Monthus and T. Garel, Phys. Rev. B **89**, 184408 (2014).
[26] M. L. Lyra, F. A. B. F. de Moura, I. N. de Oliveira, and M. Serva, Phys. Rev. E **89**, 052133 (2014).
[27] Y.-L. Xu, X. Zhang, Z.-Q. Liu, K. Xiang-Mu, and R. Ting-Qi, Eur. Phys. J. B **87**, 132 (2014).
[28] V. S. T. Silva, R. F. S. Andrade, and S. R. Salinas, Phys. Rev. E **90**, 052112 (2014).
[29] S. Boettcher, S. Falkner, and R. Portugal, Phys. Rev. A **91**, 052330 (2015).
[30] S. Boettcher and C. T. Brunson, Europhys. Lett. **110**, 26005 (2015).
[31] Y. Hirose, A. Ogushi, and Y. Fukumoto, J. Phys. Soc. Jpn. **84**, 104705 (2015).
[32] S. Boettcher and L. Shanshan, J. Phys. A **48**, 415001 (2015).
[33] A. Nandy and A. Chakrabarti, Phys. Lett. **379**, 43 (2015).
[34] S. Li and S. Boettcher, Phys. Rev. A **95**, 032301 (2017).
[35] P. Bleher, M. Lyubich, and R. Roeder, J. Math. Pures Appl. **107**, 491 (2017).
[36] H. Li and Z. Zhang, Theor. Comp. Sci. **675**, 64 (2017).
[37] S. J. Sirca and M. Omladic, ARS Math. Contemp. **13**, 63 (2017).
[38] J. Maji, F. Seno, A. Trovato, and S. M. Bhattacharjee, J. Stat. Mech. (2017) 073203.
[39] D. Andelman and A. N. Berker, Phys. Rev. B **29**, 2630 (1984).
[40] M. J. P. Gingras and E. S. Sørensen, Phys. Rev. B. **46**, 3441 (1992).
[41] G. Migliorini and A. N. Berker, Phys. Rev. B. **57**, 426 (1998).
[42] M. J. P. Gingras and E. S. Sørensen, Phys. Rev. B. **57**, 10264 (1998).
[43] C. N. Kaplan and A. N. Berker, Phys. Rev. Lett. **100**, 027204 (2008).
[44] C. Güven, A. N. Berker, M. Hinczewski, and H. Nishimori, Phys. Rev. E **77**, 061110 (2008).
[45] M. Ohzeki, H. Nishimori, and A. N. Berker, Phys. Rev. E **77**, 061116 (2008).
[46] E. Ilker and A. N. Berker, Phys. Rev. E **89**, 042139 (2014).
[47] M. Demirtaş, A. Tuncer, and A. N. Berker, Phys. Rev. E **92**, 022136 (2015).
[48] P. E. Cladis, Phys. Rev. Lett. **35**, 48 (1975).
[49] F. Hardouin, A. M. Levelut, M. F. Achard, and G. Sigaud, J. Chem. Phys. **80**, 53 (1983).
[50] J. O. Indekeu, A. N. Berker, C. Chiang, and C. W. Garland, Phys. Rev. A **35**, 1371 (1987).
[51] R. R. Netz and A. N. Berker, Phys. Rev. Lett. **68**, 333 (1992).
[52] S. Kumari and S. Singh, Phase Transitions **88**, 1225 (2015).
[53] P. Bak and R. Bruinsma, Phys. Rev. Lett. **49**, 249 (1982).
[54] A. Fukuda, Y. Takanishi, T. Isozaki, K. Ishikawa, and H. Takezoe, J. Mater. Chem. **4**, 997 (1994).
[55] A. N. Berker and L. P. Kadanoff, J. Phys. A **13**, L259 (1980).
[56] A. N. Berker and L. P. Kadanoff, J. Phys. A **13**, 3786 (1980).
[57] A. J. Bray and M. A. Moore, Phys. Rev. Lett. **58**, 57 (1987).
[58] E. J. Hartford and S. R. McKay, J. Appl. Phys. **70**, 6068 (1991).
[59] M. Nifle and H. J. Hilhorst, Phys. Rev. Lett. **68**, 2992 (1992).
[60] M. Nifle and H. J. Hilhorst, Physica A **194**, 462 (1993).
[61] M. Cieplak, M. S. Li, and J. R. Banavar, Phys. Rev. B **47**, 5022 (1993).
[62] F. Krzakala, Europhys. Lett. **66**, 847 (2004).
[63] F. Krzakala and J. P. Bouchaud, Europhys. Lett. **72**, 472 (2005).
[64] M. Sasaki, K. Hukushima, H. Yoshino, and H. Takayama, Phys. Rev. Lett. **95**, 267203 (2005).
[65] J. Lukic, E. Marinari, O. C. Martin, and S. Sabatini, J. Stat. Mech. (2006) L10001.
[66] P. Le Doussal, Phys. Rev. Lett. **96**, 235702 (2006).
[67] T. Rizzo and H. Yoshino, Phys. Rev. B **73**, 064416 (2006).
[68] H. G. Katzgraber and F. Krzakala, Phys. Rev. Lett. **98**, 017201 (2007).
[69] H. Yoshino and T. Rizzo, Phys. Rev. B **77**, 104429 (2008).
[70] J. H. Pixley and A. P. Young, Phys. Rev. B **78**, 014419 (2008).
[71] T. Aspelmeier, Phys. Rev. Lett. **100**, 117205 (2008).
[72] T. Aspelmeier, J. Phys. A **41**, 205005 (2008).
[73] T. Mora and L. Zdeborova, J. Stat. Phys. **131**, 1121 (2008).
[74] N. Aral and A. N. Berker, Phys. Rev. B **79**, 014434 (2009).
[75] Q. H. Chen, Phys. Rev. B **80**, 144420 (2009).
[76] T. Jörg and F. Krzakala, J. Stat. Mech. (2012) L01001.
[77] W. de Lima, G. Camelo-Neto, and S. Coutinho, Phys. Lett. A **377**, 2851 (2013).
[78] W. Wang, J. Machta, and H. G. Katzgraber, Phys. Rev. B **92**, 094410 (2015).
[79] V. Martin-Mayor and I. Hen, Sci. Rep. **5**, 15324 (2015).
[80] Z. Zhu, A. J. Ochoa, S. Schnabel, F. Hamze, and H. G. Katzgraber, Phys. Rev. A **93**, 012317 (2016).
[81] W. Wang, J. Machta, and H. G. Katzgraber, Phys. Rev. B **93**, 224414 (2016).
[82] J. Marshall, V. Martin-Mayor, and I. Hen, Phys. Rev. A **94**, 012320 (2016).
[83] L. A. Fernandez, E. Marinari, V. Martin-Mayor, G. Parisi, and D. Yllanes, J. Stat. Mech. (2016) 123301.
[84] A. N. Berker, Phys. Rev. B **29**, 5243 (1984).